Residual stress evaluation in welded large thin-walled structures based on eigenstrain analysis and small sample residual stress measurement

Xu, Y., Liu, H., Bao, R. & Zhang, X.

DOI 10.1016/j.tws.2018.07.049
ISSN 0263-8231

Publisher: Elsevier

Residual stress evaluation in welded large thin-walled structures based on eigenstrain analysis and small sample residual stress measurement

Yaowu XU[1], Hao LIU[2], Rui BAO[1], Xiang ZHANG[3]

[1] Institute of Solid Mechanics, Beihang University (BUAA), Beijing, 100191, P.R. China

[2] AECC Commercial Aircraft Engine Co., Ltd, Shanghai, 200241, P.R. China

[3] Faculty of Engineering, Environment and Computing, Coventry University, Coventry, CV1 5FB, UK

Corresponding author: BAO Rui; Telephone: +8610 82339223; E-mail: rbao@buaa.edu.cn

Abstract

This paper presents an evaluation method of residual stresses in large welded thin-walled structures based on eigenstrain analysis and small sample residual stress measurement. In this method, small samples containing weld and heat-affected zones are firstly cut from large thin-walled structures, then residual stress in the small samples are measured to determine the welding-induced eigenstrains using a finite element-aided inverse solution. Finally, residual stress in large thin-walled structures are evaluated based on the obtained eigenstrain distribution. The feasibility of the proposed method was validated by evaluating residual stresses in welded plates with different lengths or widths. The method was then applied to evaluating residual stress in a welded skin-stiffener panel. Good agreement between the evaluated residual stress and measurement by diffraction technique has demonstrated the practicability of the method.

Keywords: eigenstrain, inverse solution, residual stress, thin-walled structures, weld

Nomenclature

$\boldsymbol{B}$	Eigenstrain calibration coefficient matrix
$\boldsymbol{B}^{-1}$	Inverse matrix of $\boldsymbol{B}$
$\boldsymbol{B}^{\mathrm{T}}$	Transpose matrix of $\boldsymbol{B}$
B_{ij}	$\boldsymbol{B}$ matrix component representing the residual stress in the ith interval caused by a unit eigenstrain in the jth interval
$\boldsymbol{B}_{\mathrm{eva}}$	$\boldsymbol{B}$ matrix correlated to a specimen in which residual stress is to be evaluated
$\boldsymbol{B}_{\mathrm{mea}}$	$\boldsymbol{B}$ matrix correlated to a specimen in which residual stress has been measured by

	experiment
m, n	Total number of intervals of eigenstrain zone and residual stress field, respectively
$U_j(x)$	Pulse function
$\boldsymbol{\varepsilon}^*$	Eigenstrain
ε^*_y	Eigenstrain component in y direction
$\boldsymbol{\sigma}$	Residual stress
$\boldsymbol{\sigma}_{\text{eva}}$, $\boldsymbol{\sigma}_{\text{mea}}$	Residual stresses that are to be evaluated and have been measured, respectively

1. Introduction

The application of advanced welding technologies in aircraft integral metallic structures is recognized as one of the most promising methods for further cost and weight savings. However, residual stresses are introduced during a welding process and consequently influence the structural integrity assessment [1-4]. Therefore, it is important and necessary to evaluate the magnitude and distribution of residual stresses for predicting the durability and damage tolerance performance and avoiding premature failure in service, and thus promoting the integral thin-walled structures. There are two major approaches to evaluate residual stress in welded components, i.e. experimental measurement of welded structures or simulation of the welding process.

The most popular techniques for measurement of welding residual stresses include the diffraction methods and mechanical methods. Diffraction-based techniques, such as the X-ray diffraction and neutron diffraction techniques, are non-destructive means and are more accurate and automatic compared to the mechanical methods. However, the neutron diffraction technique is limited to resources and specimen size, and difficulties may arise for certain alloys due to inhomogeneous microstructure and strong and varying crystallographic texture in the welds [5, 6]. Mechanical methods are based on the strain relief principle and hence mostly destructive or semi-destructive. The hole-drilling method, the crack compliance method and the contour method are the most commonly used methods. The hole-drilling method requires commonly available equipment and is easy to operate. However, it has a limited spatial resolution and errors could arise due to localized yielding [7]. The crack compliance method improves the resolution of the residual stress variation, but the surface gauge used in the method could give weak response to the release of sub-surface stresses and might result in instability problems [8]. Nowadays, the contour method proposed by Prime and Gonzales has become more and more popular

owing to its straightforward theory and simple implementation [9]. Nevertheless, the assumption of a flat cut in the contour method is overly restrictive and misleading, which makes error minimization and correction important and necessary [10].

In addition to experimental measurement techniques, residual stresses can be evaluated by simulating the welding process using the finite element (FE) method. Joshi et al. presented a simulation of welding-induced residual stresses in a circular hollow section T-joint to explore the influential factors to the initiation and propagation of fatigue crack [11]. A sequentially coupled thermal-stress analysis was conducted by Lee et al. to model the welding process of a Y-shaped joint, and a small scale parametric study was carried out to investigate the influences of key welding parameters on the magnitude and distribution of residual stress [12]. Paulo et al. built a novel shell element FE model to simulate the friction stir welding process of building an integral stiffened panel to predict the residual stress, material softening and geometric distortion [13]. Although these simulation results were comparable with experimental measured residual stresses, the thermo-mechanical models required large number of material properties and welding process parameters. Moreover, thermo-elasto-plastic FE analysis of large complex welded structures requires high-performance computers and significant amount of computing time.

Eigenstrain is a generic name given by Mura to such nonelastic strains caused by thermal expansion, phase transformation, initial strains, plastic strains and misfit strains, and residual stresses are created owing to the incompatibility of the eigenstrains [14]. Ueda et al. proposed the concept of inherent strain as the source of residual stress and developed a general theory for evaluating residual stresses based on estimation of the inherent strain [15]. Obviously, eigenstrain has the same meaning as the inherent strain. In the following sections, the terminology given by Mura was used, i.e. the inelastic and non-compatible strains are called eigenstrain. For a welded joint, the eigenstrain consists of thermal, transformation and plastic strains induced by the welding process.

There are many advantages offered by the eigenstrain approach for evaluating the welding residual stress; once the eigenstrain distribution is deduced, the residual stress can be determined by using a linear elastic model rather than a nonlinear elasto-plastic one [16]; the eigenstrain approach enables prediction of the object's distortion and residual stress re-distribution during any subsequent machining operation [17]. Ueda et al. presented a series of work demonstrating practical applications to cases such as butt-welded joints, long welded joints, axisymmetric shaft, and T- and I-shaped joints, etc., describing a way of

determining the inherent strain and residual stress [18-21]. Hill et al. proposed a localized eigenstrain method focusing on finding residual stress only in the weld bead region of the joint, therefore the required experimental effort was greatly reduced in comparison with Ueda's method [22]. Korsunsky et al. developed a framework for predictive modelling of the residual stress due to surface peening and inertia friction welding [23-25].

This paper presents a method for evaluating residual stresses in large welded thin-walled structures based on the eigenstrain analysis and small sample residual stress measurement. In this method, residual stresses in small samples cut from large structures were measured at first, then the eigenstrain introduced by the welding process was determined using an FE-aided inverse method. Finally, residual stress in large thin-walled structures was evaluated based on the obtained eigenstrain. Two case studies were carried out to demonstrate the applicability of the presented method: residual stresses in welded plates of different lengths or widths, and residual stress distribution in a welded skin-stiffener panel.

2. Method

2.1. Procedure

Based on the postulate that a residual stress field can be uniquely determined by elastic equilibration of a distribution of eigenstrain in an object, the procedure of the presented method for evaluating residual stresses in welded large thin-walled structures involves three steps: (1) residual stresses in the small sample, which is cut from the large structure and contains the same weld and heat-affected zone, is measured using an established techniques, e.g., the diffraction method; (2) a calibration coefficient matrix denoted as $\boldsymbol{B}_{\mathrm{mea}}$ is established by performing FE analysis. The matrix is related to the small sample, in which the residual stress has been measured. Eigenstrain distribution induced by the welding process is then determined by solving linear algebraic equations relating the $\boldsymbol{B}_{\mathrm{mea}}$ matrix and the measured residual stress; (3) a calibration coefficient matrix related to the thin-walled structure, in which residual stress will be evaluated, is established by FE analysis and denoted as $\boldsymbol{B}_{\mathrm{eva}}$. Then residual stress field in the welded large thin-walled structure can be evaluated based on the obtained eigenstrain and $\boldsymbol{B}_{\mathrm{eva}}$ matrix. A flowchart of the proposed method and calculation procedure is shown in Fig. 1.

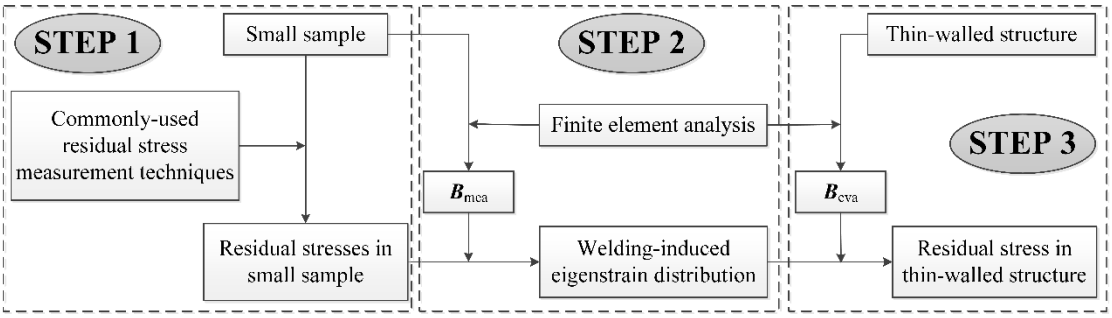

Fig. 1. Flowchart of the proposed method and calculation procedure.

In fact, the implicit limitation of the presented method is that the welds in reference samples and large actual structures must be the same, i.e. the welding process parameters and the weld dimensions in the small sample and the large thin-walled structure should be maintained the same. Considering that the transverse residual stresses (perpendicular to weld) are usually much smaller than those in the longitudinal direction (parallel to weld) in welded thin-walled structures [26], only the longitudinal residual stresses are taken into account in this paper.

2.2. Inverse solutions for eigenstrain and residual stress

Schajer's pulse method is used here in the inverse solutions for eigenstrain owing to its straightforward concept and concise algebraic operation [27-29]. In the pulse method, residual stress field and eigenstrain distribution are discretized to a series of discrete values, as shown in Fig. 2 and equation (1).

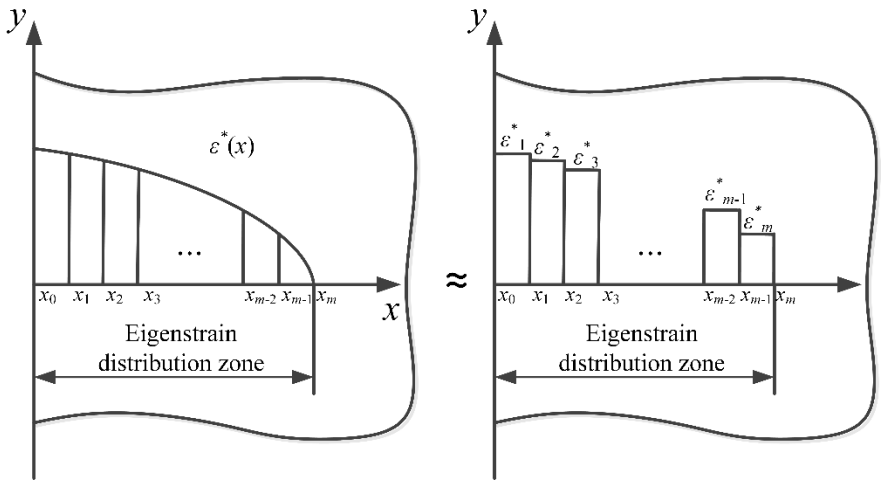

Fig. 2. Discretization of eigenstrain distribution.

$$\begin{cases} \varepsilon^*\left(x_j\right) = \sum_{j=1}^{m} \varepsilon_j^* U_j\left(x\right) \\ \sigma\left(x_j\right) = \sum_{j=1}^{n} \sigma_j U_j\left(x\right) \end{cases} \tag{1}$$

where ε^* represents the eigenstrain distribution function and ε^*_j corresponds to the eigenstrain value in the jth interval; σ represents the residual stress distribution function and σ_j corresponds to the stress value in the jth interval. $U_j(x)$ is the pulse function, m and n are the total number of intervals of eigenstrain zone and residual stress field, respectively.

The pulse functions are defined by equation (2):

$$U_j(x) = \begin{cases} 1 & x_{j-1} \le x \le x_j \\ 0 & x < x_{j-1}, x > x_j \end{cases} \tag{2}$$

Assuming a linear elastic relationship, the measured residual stresses corresponding to the eigenstrain given by Eq. (1) become

$$\boldsymbol{\sigma} = \boldsymbol{B}\boldsymbol{\varepsilon}^* \tag{3}$$

An element B_{ij} in matrix $\boldsymbol{B}$ represents the residual stress in the ith interval caused by a unit eigenstrain in the jth interval, i.e.

$$B_{ij} = \sigma(x_i)\Big|_{\varepsilon^*(x)=U_j(x)} \tag{4}$$

$\boldsymbol{B}$ is an $n \times m$ stress matrix due to applied unit eigenstrains, which is also called an eigenstrain calibration coefficient matrix and can be easily determined by FE analyses. Therefore, if residual stress distributions of small samples were determined by experimental techniques, the eigenstrain due to the welding process could be evaluated on condition that $n \ge m$. For a welded joint, n, the total number of intervals of residual stress field, is usually greater than m, the total number of intervals of eigenstrain zone, because eigenstrain zone only exists within and around the weld.

When $n = m$, we have

$$\boldsymbol{\varepsilon}^* = \boldsymbol{B}^{-1}\boldsymbol{\sigma} \tag{5}$$

If $n > m$, the solution of $\boldsymbol{\varepsilon}^*$ can be obtained by Eq. (6).

$$\boldsymbol{\varepsilon}^* = \left(\boldsymbol{B}^{\mathrm{T}}\boldsymbol{B}\right)^{-1}\boldsymbol{B}^{\mathrm{T}}\boldsymbol{\sigma} \tag{6}$$

Subscript "mea" is assigned to $\boldsymbol{B}$ and $\boldsymbol{\sigma}$ to demonstrate that these matrices are related to samples whose residual stress field has been physically measured, whereas subscript "eva" denotes that the matrices are related to structures whose residual stress is to be evaluated by analysis. Hence, calculation steps in the presented method can be expressed by following equations ($n > m$):

$$\boldsymbol{\varepsilon}^* = \left(\boldsymbol{B}_{\mathrm{mea}}{}^{\mathrm{T}}\boldsymbol{B}_{\mathrm{mea}}\right)^{-1}\boldsymbol{B}_{\mathrm{mea}}{}^{\mathrm{T}}\boldsymbol{\sigma}_{\mathrm{mea}} \tag{7}$$

$$\boldsymbol{\sigma}_{\text{eva}} = \boldsymbol{B}_{\text{eva}}\boldsymbol{\varepsilon}^{*} \tag{8}$$

2.3. Numerical demonstration

2.3.1. Specimens and the given eigenstrain distribution

An FE simulation was performed here to demonstrate the operation of the presented method. The original specimen was a rectangular plate of 100 mm × 200 mm containing a weld and a self-balanced longitudinal residual stress field that was caused by a given eigenstrain distribution expressed by Eq. (9).

$$\varepsilon^{*}_{y} = 0.001\cos(\pi x / 40),\ (-20 \le x \le 20) \tag{9}$$

where ε^{*}_{y} is the initial longitudinal eigenstrain parallel to the weld line, and x represents the distance from the weld centerline. Fig.3 shows the specimen and cutting position for a smaller sample of 100 mm × 50 mm.

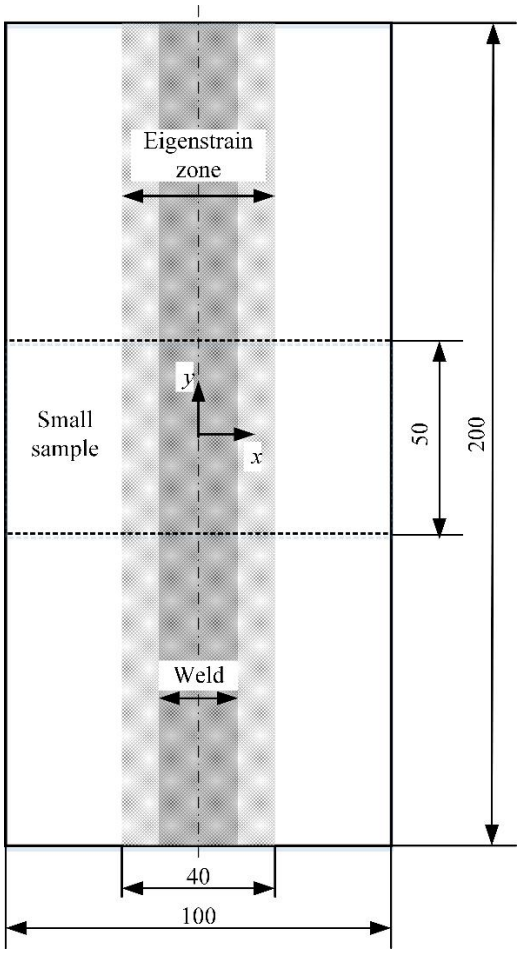

Fig. 3. Specimen configuration and dimension, and cutting position for the smaller sample (Unit: mm).

Based on the method precondition that the welds in reference samples and large actual structures must be the same, it can be considered that the through thickness variations, geometry modifications and

material properties in the welds of the small sample and large plate are the same. Therefore, the following assumptions and approximations in the linear elastic FE simulations are concise and reasonable and will not influence the accuracy of the evaluations:

- The welded plates were simplified to 2D models in the FE simulation.
- The thickness variation and geometry modification due to the weld were neglected by the FE model.
- The material properties within and around the welds were considered the same as that of the base material.

Taking into account of the symmetrical characteristic of the specimen and eigenstrain distribution, a 2D model of one-quarter plate was built using the ANSYS commercial FE code and a 50 × 100 mesh of high-order 8-node quadrilateral plane stress elements (PLANE183). The material behavior was assumed to be isotropic and linear elastic with a Young's modulus of 78 GPa and a Poisson's ratio of 0.33. The eigenstrain was inputted to the model by the command "INISTATE", and the model was then solved to ensure that it was self-balanced. The eigenstrain distribution and the residual stress in the specimen are shown in Fig. 4. It is observed that residual stress distribution changes direction at the boundary of the eigenstrain zone, which gives us idea to determine the boundary of the eigenstrain zone in the following work. The cutting process of the small sample, as shown in Fig. 3, was simulated by removing those elements that were outside the small sample's boundaries as indicated by dotted lines. The self-balanced residual stress in the small sample, for the comparison purpose, is also shown in Fig. 4, which was subsequently used as a known initial condition for evaluating the residual stress in the original large specimen.

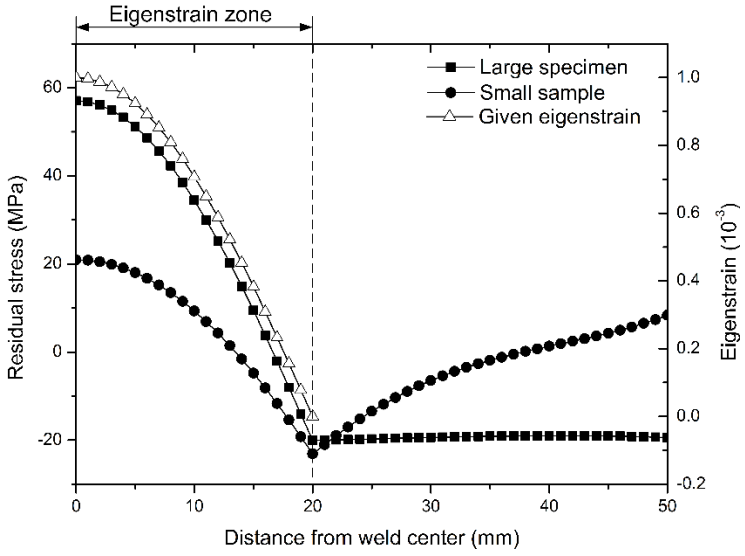

Fig. 4. Given eigenstrain and calculated residual stress distribution in the large specimen and small sample (corresponding to the specimen configurations in Fig. 3).

2.3.2. Residual stress evaluation in the large specimen using the proposed method

Firstly, eigenstrain was assumed to distribute in the [0, 20] mm zone according to the location where residual stress distribution in the small sample changed direction (Fig. 4). The interval length was designated as 1 mm and hence $\boldsymbol{B}_{\text{mea}}$ is a 50×20 matrix. Secondly, a 2D FE model was built for one-quarter of the small sample with the element size of 1 mm. A unit tension strain was applied at each of the intervals located within the [0, 20] mm zone, one at a time, and the corresponding residual stresses were calculated and extracted to make up the different columns in the corresponding matrix $\boldsymbol{B}_{\text{mea}}$. Fig. 5(a) shows that a unit tension strain was applied at the seventh interval. The residual stresses extracted from the path at the bottom edge were exactly the seventh column, i.e., B_{j7} ($1 \leq j \leq 50$) in matrix $\boldsymbol{B}_{\text{mea}}$, as shown in Fig. 5(b). Thirdly, the eigenstrain distribution can be obtained by solving Eq. (7), and Fig. 5(c) shows the comparison between the calculated eigenstrain and the initial given eigenstrain (Eq. (9)). The final step involves determining matrix $\boldsymbol{B}_{\text{eva}}$, and then evaluating the residual stresses in the original large specimen using Eq. (8). Evaluated residual stress distribution is compared with the residual stress obtained from FE simulations, as shown in Fig. 5(d).

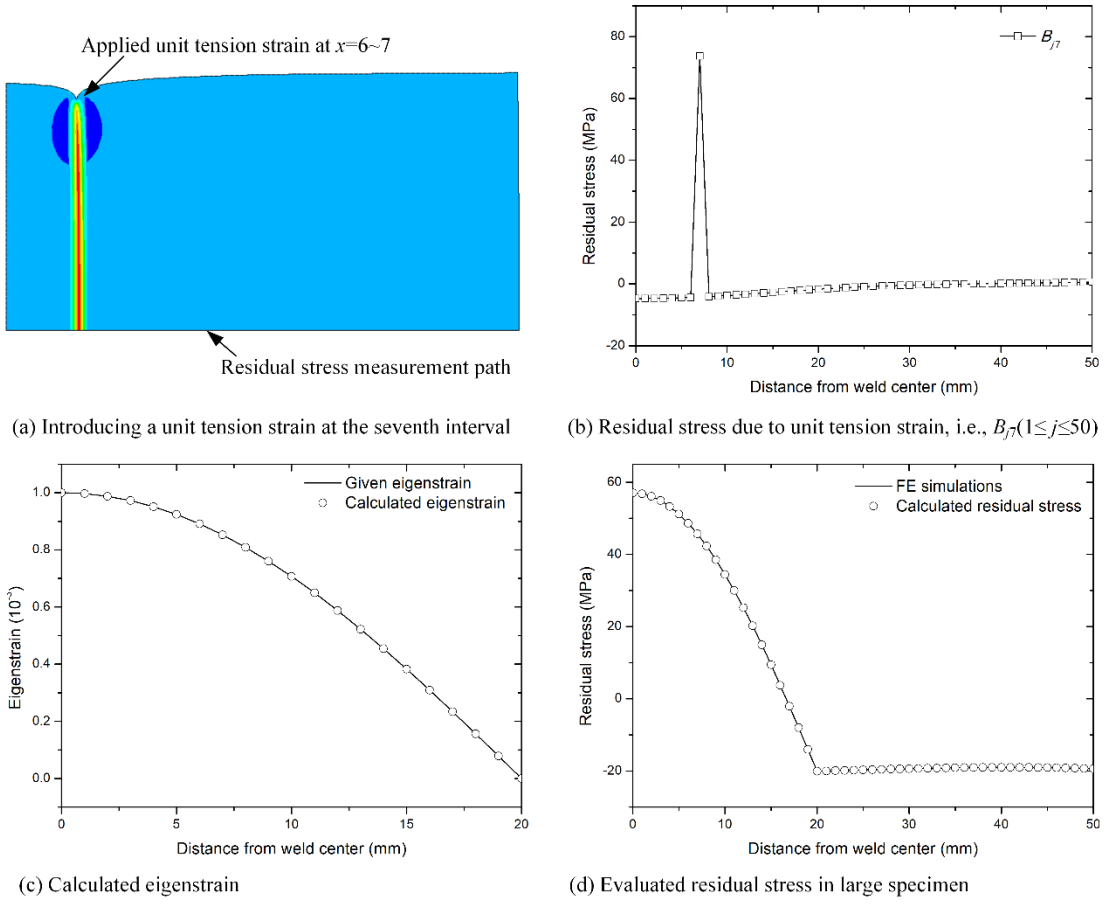

(a) Introducing a unit tension strain at the seventh interval

(b) Residual stress due to unit tension strain, i.e., $B_{j7}(1 \le j \le 50)$

(c) Calculated eigenstrain

(d) Evaluated residual stress in large specimen

Fig. 5. Residual stress evaluation process for the original large specimen.

2.3.3. Influence of eigenstrain zone boundary selection on eigenstrain evaluation

In engineering practice, the boundary of the eigenstrain zone is usually difficult to determine exactly, because the selection of a certain location where residual stress distribution changes direction is ambiguous (examples of measured residual stresses of welded plates can be found in Section 3.1.1). Therefore, exploring the influence of the eigenstrain zone boundary selection on evaluated eigenstrain is important and necessary. In this part, eigenstrain is assumed to distribute in three different zone lengths, [0, 15], [0, 20] and [0, 25] mm, and the calculated eigenstrain distributions are shown in Fig. 6.

When the eigenstrain is assumed to distribute in the [0, 15] mm zone, i.e. the assumed eigenstrain zone is located within the actual eigenstrain zone, there are significant differences between the calculated eigenstrain values and the given eigenstrains. On the contrary, when the eigenstrain is assumed to distribute in the [0, 25] or [0, 20] mm zone, i.e. the actual eigenstrain zone is located within the assumed eigenstrain zone, the calculated eigenstrain values are in good agreement with the given eigenstrains. In conclusion, inverse solutions are insensitive to the choice of the length of the assumed eigenstrain zone,

provided it exceeds the physical boundary of the actual eigenstrain zone. Therefore, the assumed eigenstrain zone should be sufficiently large to include the entire possible distance, beyond which the measured residual stress distribution changes direction.

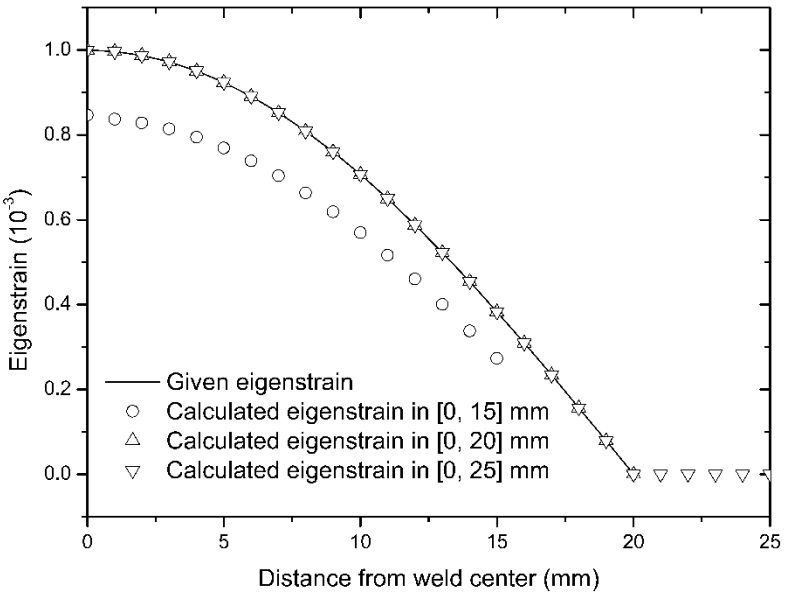

Fig. 6. Calculated eigenstrain distributions according to different eigenstrain zone boundaries.

3. Case studies with the proposed evaluation method

3.1. Residual stress in butt welded plates

3.1.1. Specimens and residual stresses

Because of the availability of measured residual stresses, a friction stir welded butt joint of aluminum alloy AA7449 plate and a pulsed metal-inert gas butt welded S355 plate [30] are used here for the validation of the proposed method. In both welds, residual stress was measured repeatedly in the same location as the plates were progressively and symmetrically shortened or narrowed by removing an equal amount of length or width from each end or side. Specimen configuration and cutting positions are shown in Fig. 7. Residual stress distributions measured using the synchrotron X-ray diffraction technique are shown in Fig. 8.

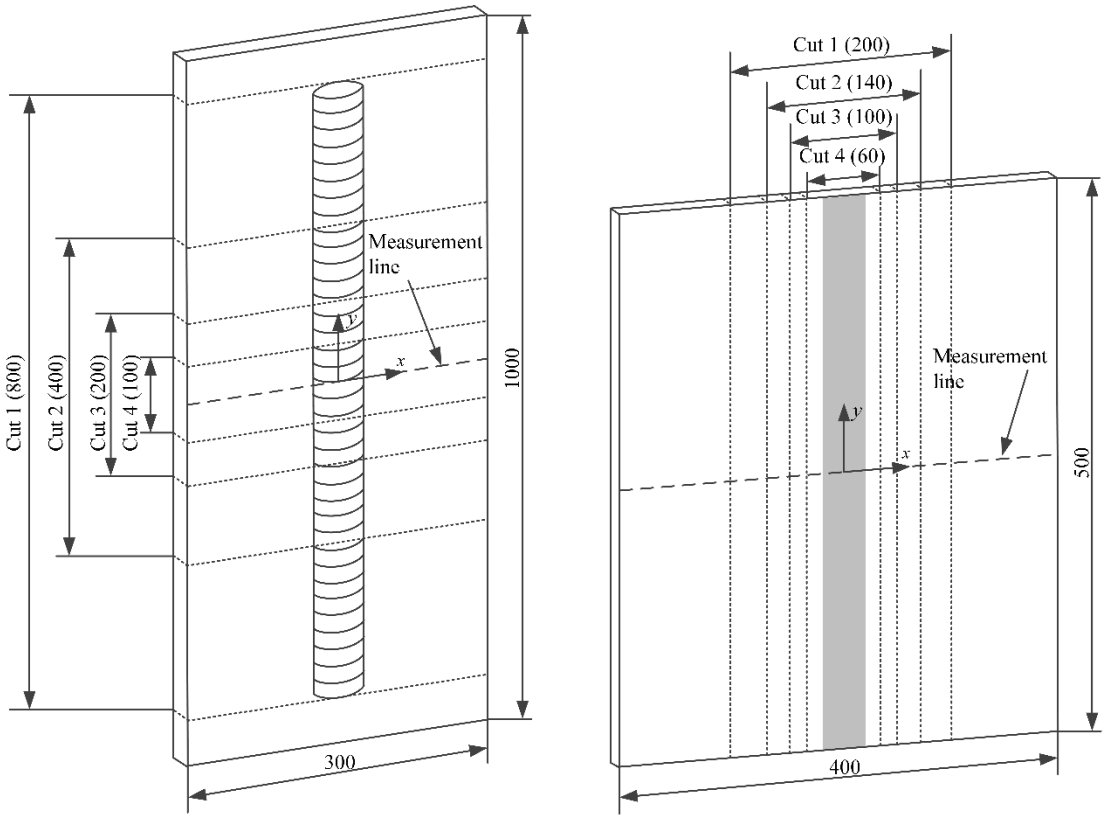

(a) Friction stir welded ΑΑ7449 plate (b) Pulsed metal-inert gas welded S355 plate

Fig. 7. Specimen configuration and extracted test pieces. (Reproduced from [30], unit: mm)

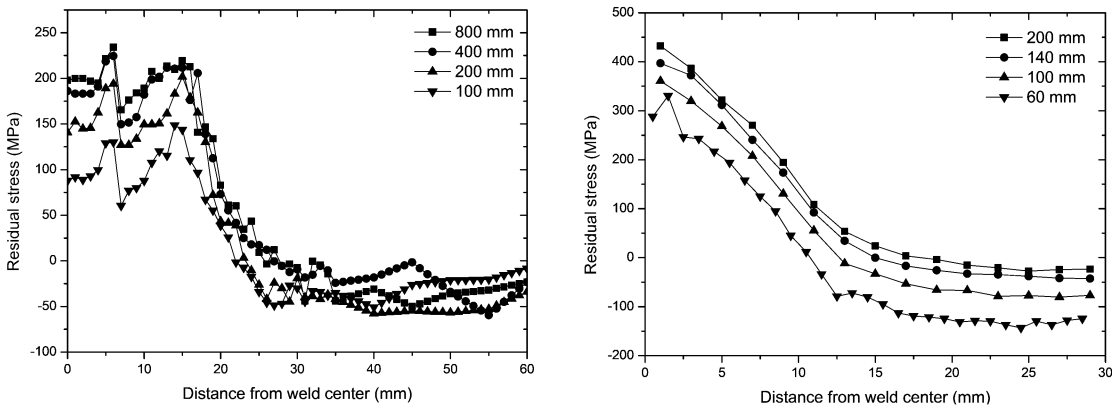

(a) Friction stir welded AA7449 plate in different lengths (b) Pulsed metal-inert gas welded S355 plate in different widths

Fig. 8. Residual stress distributions in welded plates in different lengths and widths. (corresponding to the configurations in Fig. 7. Reproduced from [30])

3.1.2. Results and discussion

In this section, residual stress distributions in specimens of different lengths or widths were evaluated based on eigenstrain distribution derived from another specimen cut from the same original plate with

measured residual stress distributions. Eigenstrain was assumed to distribute in [0, 35] mm zone in the AA7449 plates and [0, 25] mm zone for the S355 plates, according to the location where residual stress distributions changed direction. Eigenstrain distributions calculated from residual stress distributions in different lengths or widths are shown in Fig. 9.

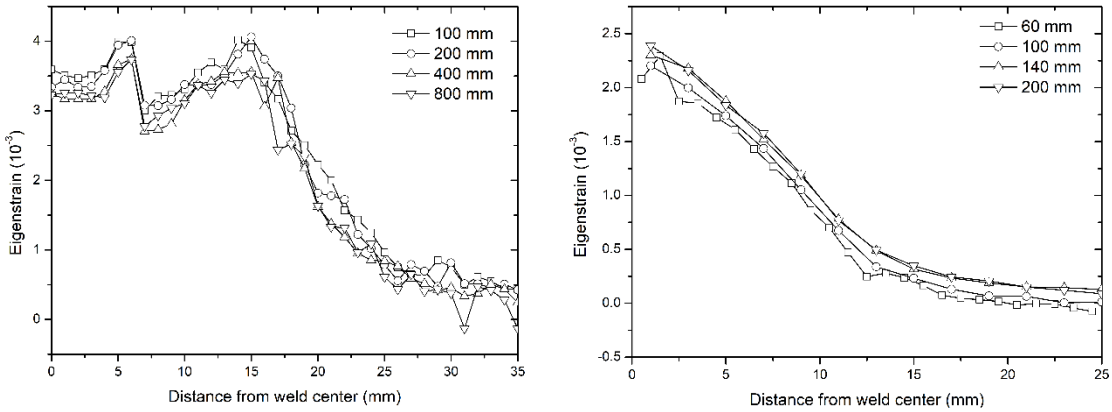

(a) Friction stir welded AA7449 plate (b) Pulsed metal-inert gas welded S355 plate

Fig. 9. Eigenstrain distributions derived from residual stresses in specimens of different lengths or widths.

The trends of eigenstrain distributions in different lengths/widths of specimens display consistently and were similar to that of the measured residual stress. Small deviations appear in the magnitude due to measurement errors in residual stresses. Furthermore, eigenstrain values gradually approach zero at approximately 35 mm and 25 mm from the weld center in AA7449 plates and S355 plates, respectively, which means that the assumptions of the widths of eigenstrain distribution zones are reasonable. Residual stress distributions calculated using the obtained eigenstrain data are shown in Figs. 10 and 11.

For pulsed metal-inert gas welded S355 plates, calculated stress results are in good agreement with the measured residual stresses in most areas. For friction stir welded AA7449 plates, the total range was divided into two sections based on the existence of eigenstrain. In Section [0, 35] mm, which is also called an eigenstrain zone, both trend and magnitude of the evaluated residual stress agree well with the measured data; In Section [35, 60] mm, which is also called a non-eigenstrain zone, however, differences appear in trend or magnitude between the calculated residual stress and measured results, particularly in the case that evaluating residual stresses in the specimen with 400 mm length. The differences arise partially from the measurement error of residual stress and partially from the inverse solution used in the proposed method: the eigenstrain theory focuses on the characterization of residual stress in the eigenstrain zone, leaving the trend of residual stress in the non-eigenstrain zone to be neglected. It sounds

acceptable because the critical factor contributing to fatigue and fracture problems of weldments is tensile residual stress within and around the weld, rather than compressive residual stress far away from the weld.

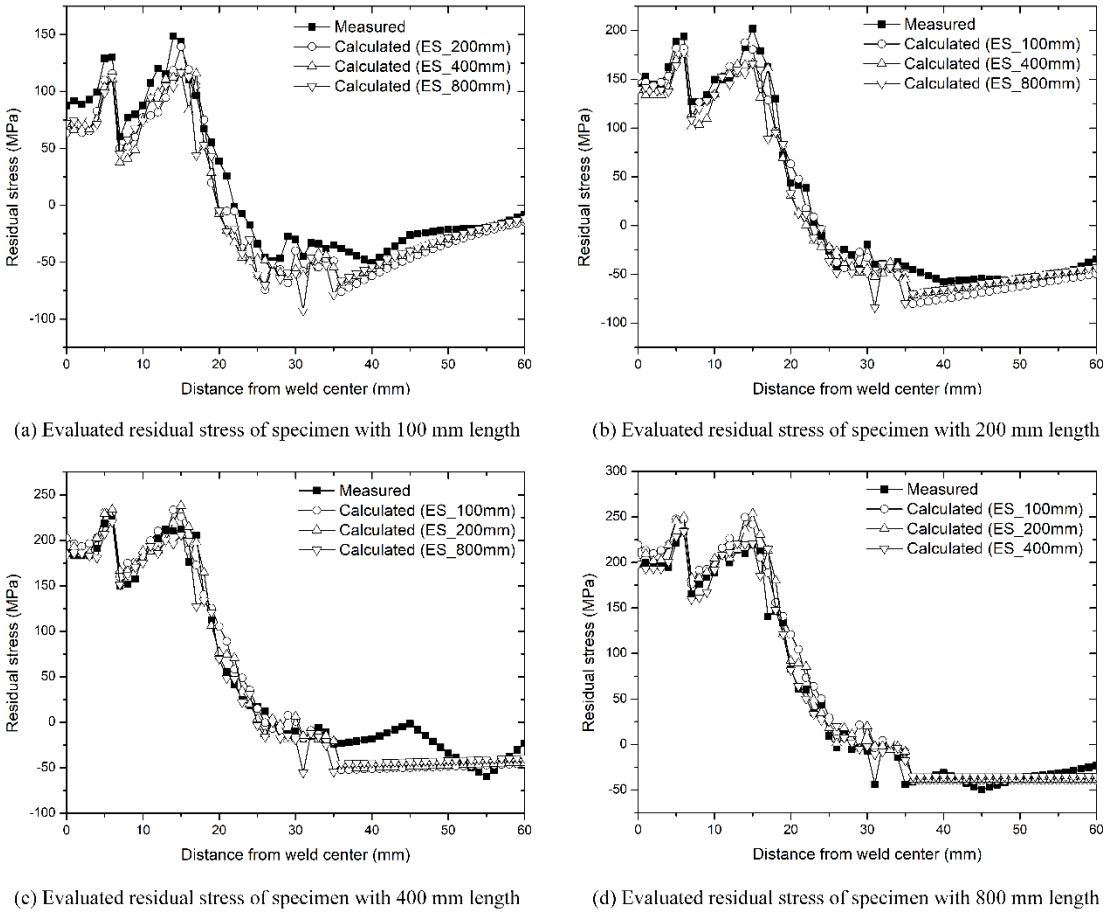

(a) Evaluated residual stress of specimen with 100 mm length

(b) Evaluated residual stress of specimen with 200 mm length

(c) Evaluated residual stress of specimen with 400 mm length

(d) Evaluated residual stress of specimen with 800 mm length

Fig. 10. Evaluated residual stress distributions in friction stir welded AA7449 specimens of different lengths. (ES: calculation was based on derived eigenstrain)

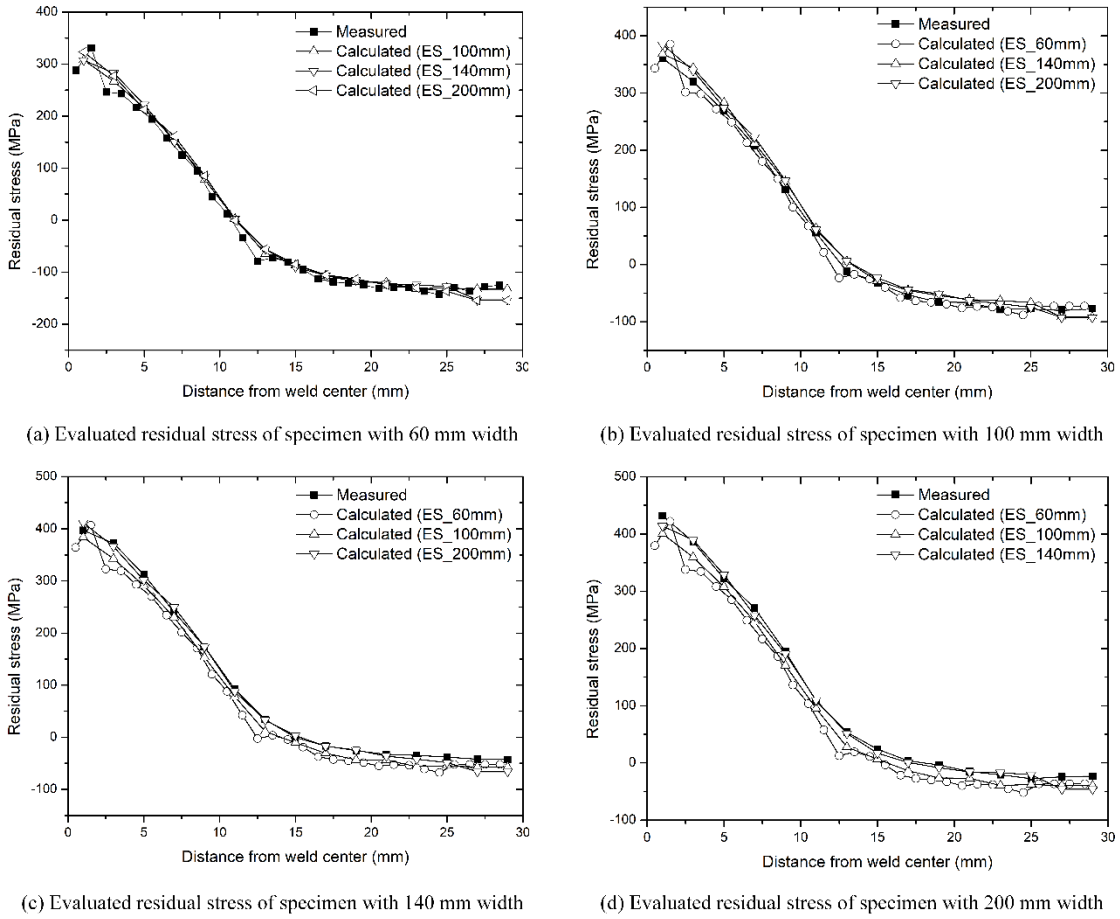

Fig. 11. Evaluated residual stress distributions in pulsed metal-inert gas welded S355 specimens of different widths. (ES: calculation was based on derived eigenstrain)

3.2. Residual stress evaluation in a welded stiffened panel

3.2.1. Specimens and residual stresses

A friction stir butt welded 2024-T351 plate is used as the small sample in the proposed method to evaluate the residual stress in a butt welded 2024-T351 stiffened panel, which was fabricated by the same welding process: The welding tool had a shoulder of 12 mm diameter; process parameters were a rotation rate of 600 rpm and a traverse speed of 100 mm/min. The welded plate had a thickness of 5 mm and consisted of two parent metal plates of 100 mm×50 mm that were joined by a friction stir weld along the long edge. The stiffened panel had a length of 200 mm and the specimen configuration is shown in Fig. 12. Residual stress distributions in the welded plate and stiffened panel were measured by the X-ray diffraction technique and are shown in Fig. 13.

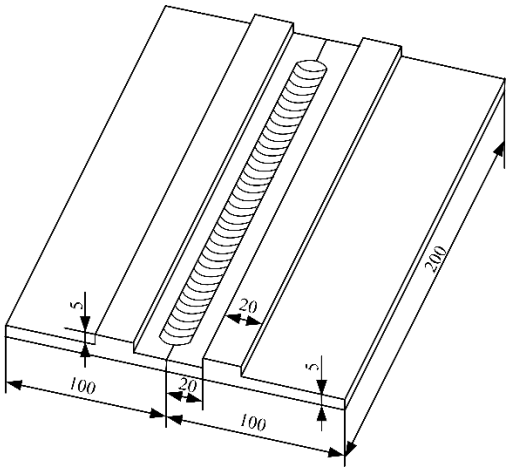

Fig. 12. Friction stir welded 2024-T351 stiffened panel. (Unit: mm)

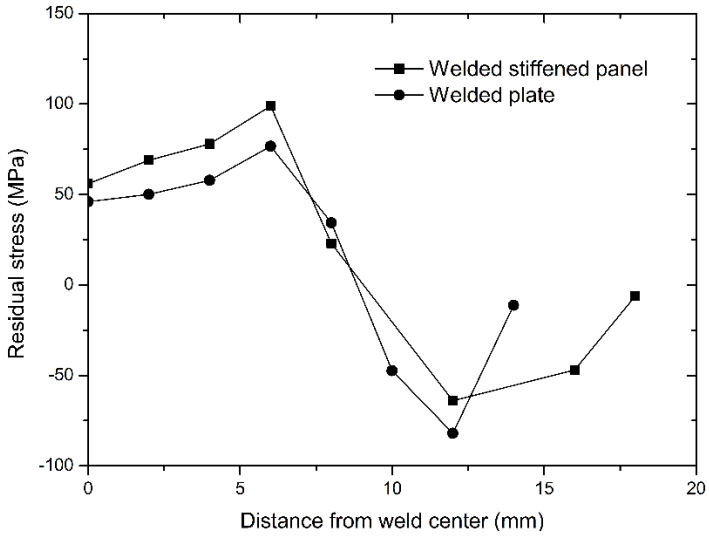

Fig. 13. Residual stress distributions in the welded plate and stiffened panel.

3.2.2. Results and discussion

At first, an eigenstrain distribution was assumed in the [0, 14] mm zone according to the location where the residual stress in the small welded plate changed direction. The eigenstrain distribution in the welded plate calculated by Eq. (7) is shown in Fig. 14. The evaluated residual stress in the welded stiffened panel is shown in Fig. 15, accompanied by comparison with the measured result using the X-ray diffraction technique. The welded stiffened panel was modelled by 3D solid elements, i.e. the 20-node high-order hexahedral element (SOLID186), in the FE simulation using ANSYS software.

In the region of [0, 12] mm, the trend of the residual stress distribution is modelled correctly. Slight differences in the stress magnitude appear due to the measurement error of the residual stress in the welded plate. However, considerable difference between the evaluated residual stress and measurement

result is shown in the region of [12, 18] mm. In addition to errors in the measurement, the disagreement can be attributed to the limitation of the presented method: the eigenstrain theory focuses on the characterization of residual stress in the eigenstrain zone and neglects the trend of residual stress beyond the eigenstrain zone.

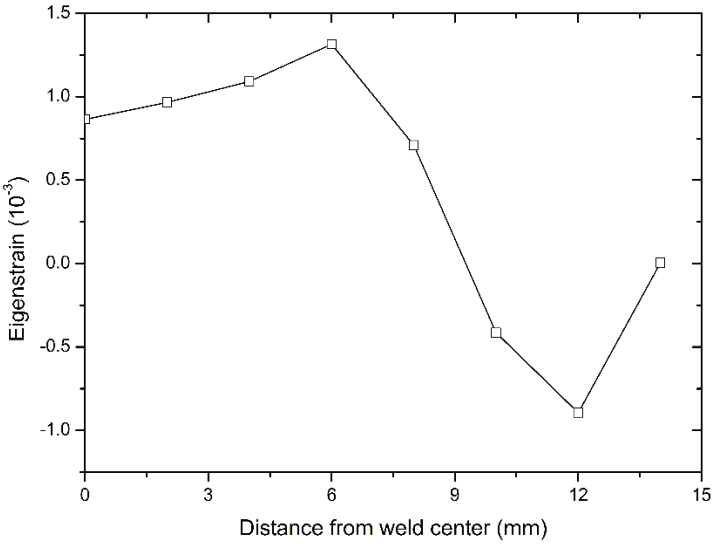

Fig. 14. Calculated eigenstrain distribution in the small welded plate.

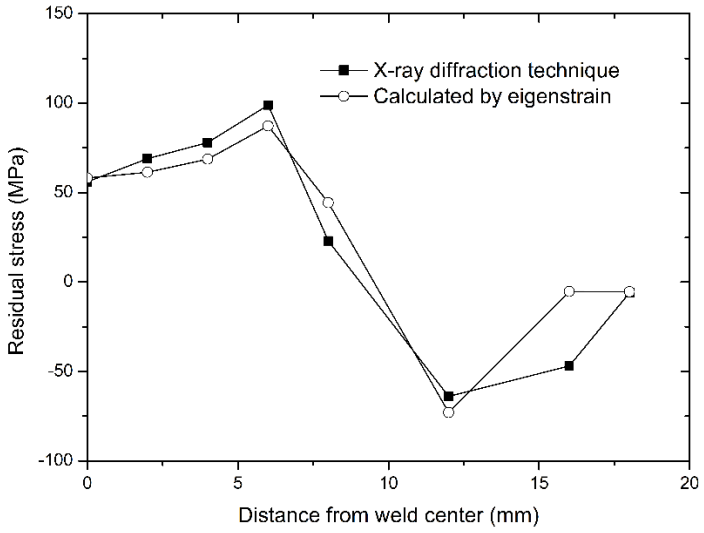

Fig. 15. Evaluated residual stress in the welded stiffened panel.

4. Conclusions

This paper presents a novel method for evaluating residual stresses in large thin-walled structures based on eigenstrain analysis and small sample residual stress measurement. The proposed method was validated by test measurement of residual stresses in welded plates of various lengths and widths, and also verified by measured residual stresses in a butt welded stiffened panel. Based on the work, following

conclusions can be drawn:

1. Inverse solutions of eigenstrain are insensitive to the choice of assumed eigenstrain zone size, provided that it exceeds the physical extent of the actual eigenstrain zone. As a good estimation, the assumed eigenstrain zone should be large enough to include the entire possible area where the measured residual stress distribution changes direction.
2. Residual stresses of butt welded plates in different lengths or widths evaluated by the proposed method are in good agreement with synchrotron X-ray diffraction measurement.
3. Residual stress distribution in the butt welded stiffened panel is modelled correctly by the presented method in terms of the distribution trend and stress magnitude compared with the measurement result using the X-ray diffraction technique. Difference in the stress values is caused partially by the measurement error of the residual stress in the welded plate and partially owing to the limitation of the eigenstrain theory used in the presented method.
4. The proposed method can be a powerful tool for evaluating residual stress distributions in large welded thin-walled structures. However, the applicability of the proposed method to cases of different thicknesses and/or weld dimensions between samples and structures still needs further investigation.

Acknowledgements

This work was supported by the National Natural Science Foundation of China [grant numbers 11272029 and 11672012].

References

[1] Bussu, G., & Irving, P. E. (2003). The role of residual stress and heat affected zone properties on fatigue crack propagation in friction stir welded 2024-t351 aluminium joints. *International Journal of Fatigue, 25*(1), 77-88.

[2] Edwards, L., Fitzpatrick, M. E., Irving, P. E., Sinclair, I., Zhang, X., & Yapp, D. (2006). An integrated approach to the determination and consequences of residual stress on the fatigue performance of welded aircraft structures. *Journal of ASTM International, 3*(2), 17.

[3] Servetti, G., & Zhang, X. (2009). Predicting fatigue crack growth rate in a welded butt joint: The role of effective R ratio in accounting for residual stress effect. *Engineering Fracture Mechanics*, *76*(11), 1589-1602.

[4] Xu, Y., Bao, R., Liu, H., & Zhang, X. (2017). A modified loading method for separating the effect of

residual stress on fatigue crack growth rate of welded joints. *Fatigue & Fracture of Engineering Materials & Structures*, *40*, 1227-1239.

[5] Ganguly, S., Fitzpatrick, M. E., & Edwards, L. (2006). Use of neutron and synchrotron X-ray diffraction for evaluation of residual stresses in a 2024-T351 aluminum alloy variable-polarity plasma-arc weld. *Metallurgical and Materials Transactions A*, *37*(2), 411-420.

[6] Bao, R., & Zhang, X. (2010). An inverse method for evaluating weld residual stresses via fatigue crack growth test data. *Engineering Fracture Mechanics*, *77*(16), 3143-3156.

[7] Withers, P. J., & Bhadeshia, H. K. D. H. (2001). Residual stress. Part 1–measurement techniques. *Materials science and Technology*, *17*(4), 355-365.

[8] Prime, M. B. (1999). Residual stress measurement by successive extension of a slot: the crack compliance method. *Applied Mechanics Reviews*, *52*, 75-96.

[9] Prime, M., & Gonzales, A. (2000). *The contour method: simple 2-D mapping of residual stresses* (No. LA-UR-00-1900). Los Alamos National Lab., NM (US).

[10] Prime, M. B., & Kastengren, A. L. (2011). The contour method cutting assumption: error minimization and correction. *Experimental and Applied Mechanics, Volume 6*, 233-250.

[11] Joshi, S., Semetay, C., Price, J. W., & Nied, H. F. (2010). Weld-induced residual stresses in a prototype dragline cluster and comparison with design codes. *Thin-Walled Structures*, *48*(2), 89-102.

[12] Lee, C. K., Chiew, S. P., & Jiang, J. (2012). Residual stress study of welded high strength steel thin-walled plate-to-plate joints part 2: Numerical modeling. *Thin-Walled Structures*, *59*, 120-131.

[13] Paulo, R. M. F., Carlone, P., Paradiso, V., Valente, R. A. F., & Teixeira-Dias, F. (2017). Prediction of friction stir welding effects on AA2024-T3 plates and stiffened panels using a shell-based finite element model. *Thin-Walled Structures*, *120*, 297-306.

[14] Mura, T. (2013). *Micromechanics of defects in solids*. Springer Science & Business Media.

[15] Ueda, Y., Fukuda, K., Nakacho, K., & Endo, S. (1975). A new measuring method of residual stresses with the aid of finite element method and reliability of estimated values. *Journal of the Society of Naval Architects of Japan*, *1975*(138), 499-507.

[16] Chien, C. H., Chen, H. J., & Chiou, Y. T. (1989). The Estimation of Welding Residual Stresses by Using Simulated Inherent Strains. *Transactions of the Japan Welding Society*, *20*(1), 52-59.

[17] Korsunsky, A. M., Regino, G. M., & Nowell, D. (2007). Variational eigenstrain analysis of residual stresses in a welded plate. *International Journal of Solids and Structures*, *44*(13), 4574-4591.

[18] Ueda, Y., & Yuan, M. G. (1993). Prediction of residual stresses in butt welded plates using inherent strains. *Journal of Engineering Materials and Technology*, *115*(4), 417-423.

[19] Ueda, Y., Fukuda, K., & Fukuda, M. (1980). A Measuring Theory of Three Dimensional Residual Stresses in Long Welded Joints. *Journal of the Japan Welding Society*, *49*(12), 845-853.

[20] Ueda, Y., Fukuda, K., & Kim, Y. C. (1986). New measuring method of axisymmetric three-dimensional residual stresses using inherent strains as parameters. *Journal of Engineering Materials and Technology*, *108*(4), 328-334.

[21] Ueda, Y., & Yuan, M. G. (1992). Prediction of welding residual stresses in T and I joints using inherent strains. 3rd report: Method for prediction of welding residual stress using residual stress generation source. *Welding international*, *6*(4), 263-269.

[22] Hill, M. R., & Nelson, D. V. (1998). The localized eigenstrain method for determination of triaxial residual stress in welds. *ASME-PUBLICATIONS-PVP*, *373*, 397-404.

[23] Korsunsky, A. M. (2005). The modelling of residual stresses due to surface peening using eigenstrain distributions. *The Journal of Strain Analysis for Engineering Design*, *40*(8), 817-824.

[24] Korsunsky, A. M. (2006). Residual elastic strain due to laser shock peening: modelling by eigenstrain distribution. *The Journal of Strain Analysis for Engineering Design*, *41*(3), 195-204.

[25] Korsunsky, A. M., Regino, G. M., Nowell, D., Karadge, M., Grant, B., Withers, P. J., ... & Baxter, G. (2009). Inertia friction welds between nickel superalloy components: analysis of residual stress by eigenstrain distributions. *The Journal of Strain Analysis for Engineering Design*, *44*(2), 159-170.

[26] Staron, P., Kocak, M., Williams, S., & Wescott, A. (2004). Residual stress in friction stir-welded Al sheets. *Physica B: Condensed Matter*, *350*(1), E491-E493.

[27] Schajer, G. S., & Prime, M. B. (2006). Use of inverse solutions for residual stress measurements. *Journal of engineering materials and technology*, *128*(3), 375-382.

[28] Schajer, G. S. (1988). Measurement of non-uniform residual stresses using the hole-drilling method. Part I—Stress calculation procedures. *Journal of engineering materials and technology*, *110*(4), 338-343.

[29] Xu, Y., & Bao, R. (2017). Residual stress determination in friction stir butt welded joints using a digital image correlation-aided slitting technique. *Chinese Journal of Aeronautics*, *30*(3), 1258-1269.

[30] Altenkirch, J., Steuwer, A., Peel, M. J., & Withers, P. J. (2009). The extent of relaxation of weld residual stresses on cutting out cross-weld test-pieces. *Powder Diffraction*, *24*(S1), S31-S36.